Heat Transfer from Boundary Layers Undergoing an Acceleration Induced Reverse Transition

ELIYAHU TALMOR and NORMAN WEBER

Rocketdyne, A Division of North American Rockwell Corporation, Canoga Park, California

An experimental and analytical investigation of heat transfer in an acceleration induced transitional flow regime is presented. A previously developed criterion for the onset of reverse transition of turbulent boundary layers is combined with a theory of forward transition to derive the effect of free-stream turbulence intensity on the critical value of an acceleration parameter for two initial velocity profiles within the turbulent boundary layer. The results are consistent with experimental observations.

Local heat transfer measurements were obtained along converging walls of rectangular flow channels having convergence angles of 45, 60, and 70 deg. Free-stream turbulence (1.6 to 11%) was induced by grids upstream of the start of convergence, and the local Reynolds number were varied by variation in channel size and stagnation pressures (200 to 500 lb./sq.in. abs.) at a gas stagnation temperature of 1,500°R.

The results indicate a two-stage reverse transition process along the converging wall with a forward transition between the two stages of reverse transition. The local Nusselt numbers obtained over a wide range of an acceleration parameter are correlated with the local Reynolds number, the acceleration parameter at the start of convergence, and the local flow area contraction ratio. The correlation is in the form of laminarization paths having negative slopes for $(N_{Nu})_r/(N_{Pr})^{0.4}$ vs. $(N_{Re})_r$ at common area ratios. Local values of free-stream turbulence intensity are required for proper application of the reverse transition criterion in conjunction with the heat transfer correlation presented.

Considerable experimental and analytical efforts have been expended for proper prediction of convective heat transfer coefficients in rapidly accelerating flows. A fair degree of success prevails if the boundary layer is either turbulent (*1, 2*) or laminar (*3*). However, recent investigations at high rates of acceleration indicate that the boundary layer may be turbulent at the start of convergence but reverts to a transitional or near laminar state toward the sonic point (*4, 5*). The process of reverse transition is seldom complete; that is, truly laminar heat transfer levels are seldom realized.

For the transitional flow regime (between the turbulent and laminar with characteristics of neither), the velocity profile within the boundary layer and its associated shear stress relation cannot be described in a universal manner. Therefore, predictions of heat transfer coefficients for this flow regime are lacking, so that emphasis has to be placed on experimental or visual observations.

The observed reduction in rocket nozzle heat transfer below that typical of a turbulent boundary layer (through the process of reverse transition) provides a strong motive to seek a method by which the phenomenon of reverse transition can be incorporated into design criteria. Two basic problems are involved: prediction of the onset of reverse transition (or laminarization) of a turbulent boundary layer, and estimation of heat transfer coefficients in the transitional flow regime.

Several basic experimental investigations of acceleration induced reverse transition of turbulent boundary layers have been reported (*6* to *9*). However, the boundary layers investigated were developed on straight, nonconverging, side plates with the stream-by-stream pressure gradient being controlled by adjustments of an opposite converging wall. Such data are hardly applicable for the design of converging walls. This is well reflected by comparisons of the effect of hot gas acceleration rate on film cooling effectiveness on nonconverging and converging walls. For the former (*10*), the film cooling effectiveness along a straight, nonconverging wall was mildly affected by the convergence angle of the opposing wall. However, recent investigations of film cooling along converging walls (*11*) indicate a drastic effect of convergence angle on film cooling effectiveness leading to a different type of correlation. A similar trend without film cooling may certainly be expected. Therefore, the design of converging walls calls for data obtained on converging walls.

To the degree that such data are available (*5, 12*), they are restricted to relatively large axisymmetric nozzles at relatively low stagnation pressures (30 to 250 lb./sq.in.abs.). Furthermore, the experimental conditions involved were unrealistically ideal; that is, the effects of free-stream turbulence at the start of convergence were eliminated by separating the combustion chamber from the test section with a large calming section in between. In compact combustion chambers, where steep convergence angles are desirable, an offsetting effect of combustion induced turbulence on the onset of reverse transition may be expected to prevail at least during the early part of convergence.

Another complicating factor is the diversification in the effect of pressure gradient (for example, convergence angle) on heat transfer (*2, 4*). At the lower Reynolds numbers range, an increase in pressure gradient tends to suppress the heat transfer rate through the phenomenon of complete or partial laminarization, while at the higher Reynolds number range an increase in heat transfer rate is thereby realized (*13, 14*). In between is a range of Reynolds numbers where the pressure gradient has no effect on heat transfer (*15*). The exact specifications of these ranges of Reynolds numbers require experimental and analytical consideration of simultaneous effects of

Eliyahu Talmor is with Shell Development Company, Emeryville, California. Norman Weber is at Montana State University, Bozeman, Montana.

free-stream turbulence, mass velocity, and pressure gradient.

It was against this background that the present investigation was undertaken. Its main objective was to generate transitional heat transfer data for plane converging walls in presence of free-stream turbulence at the start of convergence. However, to make such data useful for design purposes, the designer has to ensure the onset of reverse transition. To this end, a previously developed criterion for the onset of reverse transition was extended to include the offsetting effect of the local free-stream turbulence.

ANALYTICAL CONSIDERATIONS

The analytical treatment of heat transfer from a transitional boundary layer with variable free-stream velocity and wall temperature has met little success. The usual procedure for solving the integral momentum equation involves two prerequisites: a relation between the wall shear stress and one (or more) of the local integral parameters, and a relation between shear stress and heat transfer. Neither relation can be universally described for a transitional boundary layer.

The other approach of solving the energy equation directly is somewhat more attractive in this case as it involves just one prerequisite, that is, a relation between the surface heat flux and the energy thickness of the boundary layer. This approach was followed by Ambrok (*16*) to obtain a generalized solution for the local Nusselt number along a wall with longitudinally varying temperature and free-stream velocity.

Ambrok's solution (*16*) may be applied for calculations of laminar, transitional, and turbulent boundary layers provided that an expression of the form $(N_{Nu})_x = C(N_{Re})_x^n$ for a flat plate at constant temperature without acceleration is known for the corresponding flow regime. Such information is seldom available for a transitional boundary layer. Indeed, to develop a solution for an accelerated transitional boundary layer with variable wall temperature, Ambrok had to conduct a separate experimental investigation of heat transfer in the transitional regime along an isothermal flat plate without acceleration.

Another drawback of the method is the implicit assumption that C and n are not affected by acceleration and variable wall temperature. This is not fully supported by experimental data. For example, Ambrok's experimental results for a nonaccelerated transitional boundary layer along an isothermal plate indicate that $C = 0.188$ and $n = 0.6$ for $(N_{Re})_x < 2(10^5)$ and $C = 0.000386$ and $n = 1.11$ for $(N_{Re})_x > 2(10^5)$. However, recent results (*11*) for accelerated flow along a wall at a convergence angle of 60° with free-stream turbulence intensities of 6.4 to 10% at the start of convergence indicate $C = 0.330$ and $n = 0.6$ for $(N_{Re})_x < 4(10^5)$ and $C = 0.00118$ and $n = 1.04$ for $(N_{Re})_x > 4(10^5)$. While the values of n are consistent, their range of applicability is different, and the values of C are markedly apart. Thus, to develop a solution or a design correlation for heat transfer to converging walls in the transitional laminarized flow regime, there seems to be no escape from experiments under the actual or simulated conditions of acceleration, free-stream turbulence, and wall cooling.

While the analytical treatment of heat transfer in the transitional, boundary-layer, flow regime is rather limited, improved analytical success has been encountered in predicting the onset of reverse transition of a turbulent boundary layer (*2*). This is further developed and discussed herein.

ONSET OF REVERSE TRANSITION

A criterion for the onset of reverse transition of a compressible turbulent boundary layer on an infinite wall has been derived (*2*) from the integral momentum equation written in terms of a modified Stewartson coordinate system (*17*). A one-seventh power velocity profile is assumed at the start of reverse transition, and the associated shear stress relation is substituted in the momentum equation. On the basis of the contention that the factors delaying forward transition also affect reverse transition, it is assumed (*2*) that the onset of reverse transition will occur when the momentum thickness Reynolds number is reduced (by acceleration) to the same critical value of 360 commonly used for transition in the forward direction. With the further requirement of a negative momentum thickness gradient, the onset of reverse transition is shown to occur when an acceleration parameter K_r (defined below) exceeds a critical value of $2.48(10^{-6})$; that is

$$K_r = \left(\frac{\nu_o}{U_e^2}\right)\frac{U_e}{X} > 2.48\ (10^{-6}) \qquad (1)$$

where

$$U_e = \sqrt{\frac{T_o}{T_e}}\,u_e$$

$$X = \int_0^x \frac{\rho_r \mu_r}{\rho_o \mu_o}\sqrt{\frac{T_e}{T_o}}\,dx$$

Transforming to conventional coordinates and expressing K_r in terms of the local pressure-ratio gradient, Reynolds number, and Mach number, we get

$$\frac{(P_o/P_e)}{\gamma(N_{Re})_r N^2_{Ma}}\left[-d_h\frac{d(P_e/P_o)}{dx}\right]\left(\frac{T_o}{T_r}\right)^{2m}\left[\frac{4+2N_{Ma}(\gamma-1)}{4+3N_{Ma}(\gamma-1)}\right] > 2.48(10^{-6}) \qquad (2)$$

Equation (2) is in good agreement with the experimental observations of Launder (*6*) and Moretti and Kays (*7*). However, it does not reflect the offsetting effect of the free-stream turbulence on the onset of reverse transition. This results from the use of a unique value for the critical, momentum thickness, Reynolds number. Actually, the latter is a function of the free-stream turbulence intensity and should be introduced as such into the original derivation (*2*). In this manner, allowance can be made for the effect of free-stream turbulence on the onset of reverse transition of a turbulent boundary layer.

Generalizing the reverse transition criterion in terms of a variable $(N_{Re})_{\theta,e,c}$, we have

$$K_r > \frac{0.0039}{(N_{Re})^{5/4}_{\theta,e,c}} \qquad (3)$$

for which $(N_{Re})_{\theta,e,c} = 360$ is a special case leading to Equations (1) and (2).

To describe $(N_{Re})_{\theta,e,c}$ as a function of free-stream turbulence intensity, a theory of boundary-layer transition is required which includes the combined effect of free-stream turbulence and pressure gradient on $(N_{Re})_{\theta,e,c}$. A suitable theory is that of Van Driest and Blumer (*18*). It is in good agreement with experimental results (*18, 19*) and has also been successfully used for determination of free-stream turbulence intensities from transitional heat transfer measurements (*20*).

Accordingly (*18*), the relation between the critical,

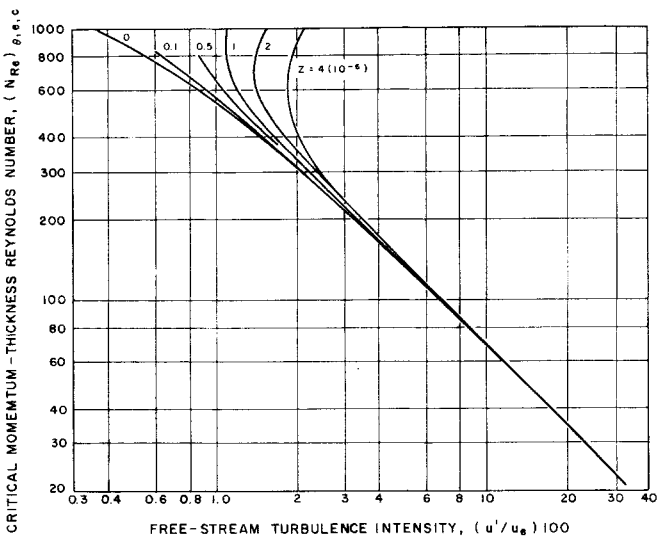

Fig. 1. Effect of free-stream turbulence and pressure gradient on forward transition of a laminar boundary layer (5).

velocity thickness, Reynolds number (for forward transition), the free-stream turbulence intensity, and the pressure gradient is of the form

$$\frac{9{,}860}{(N_{Re})_{\delta,e,c}} = 1 - 0.0485\,\Lambda + 3.36\,(N_{Re})_{\delta,e,c}\,(u'/u_e)^2 \quad (4)$$

where

$$\Lambda = \text{Pohlhausen parameter} = (-\delta^2/\mu u_e)\,(dP/dx)$$

For a laminar boundary layer (at the onset of transition), $(\delta/\theta) = 7.53$ (*21*). Substitution in Equation (4) with the notation

$$\Lambda = (N_{Re})^2_{\delta,e}(\mu_e/\rho_e u_e^2)\,(d\,u_e/d\,x) = (N_{Re})^2_{\delta,e}\,Z$$

yields

$$\frac{1{,}310}{(N_{Re})_{\theta,e,c}} = 1 - 2.75\,(N_{Re})^2_{\theta,e,c}\,Z + 25.3\,(N_{Re})_{\theta,e,c}(u'/u_e)^2 \quad (5)$$

Equation (5) was solved for $(N_{Re})_{\theta,e,c}$ vs. (u'/u_e) at various values of Z (Figure 1). As shown, the condition $(N_{Re})_{\theta,e,c} = 360$ corresponds to free-stream turbulence intensities on the order of 2%; that is, the reverse transition criterion (2) represented by Equation (1) or (2) is restricted to free-stream turbulence intensities (or turbulence intensities at the edge of the boundary layer) on the order of 2%. To obtain a reverse transition criterion over a wide range of turbulence levels, the results of Figure 1 were substituted in Equation (3), and critical values of the acceleration parameter K_r were calculated as a function of (u'/u_e). For (u'/u_e) 100 $\geq$ 3, the critical, momentum thickness, Reynolds number is independent of Z (Figure 1), so that $K_{r,c}$ could be solved uniquely in terms of the free-stream turbulence intensity. For (u'/u_e) 100 $<$ 3, where $(N_{Re})_{\theta,e,c}$ is also a function of Z, the adopted values of $K_{r,c}$ from Equation (3) were those satisfying the condition $K_{r,c} \approx Z$ at a given free-stream turbulence intensity. The results are represented by the upper curve in Figure 2 corresponding to a one-seventh power velocity profile at the onset of reverse transition.

Accordingly (Figure 2), the free-stream turbulence has a drastic offsetting effect on the onset of reverse transition of a turbulent boundary layer. While acceleration parameters lower than $1(10^{-6})$ will induce reverse transition at free-stream turbulence levels less than 1.1%, they have to be as high as 4.4 (10^{-6}) at free-stream turbulence levels on the order of 3%. Therefore, a fast decay of free-stream turbulence, prior to or during the early stage of convergence, should be highly favorable for the onset of an acceleration induced laminarization of a turbulent boundary layer.

Also shown in Figure 2 are similar results for a lower power initial velocity profile. This curve was generated through a further generalized form of Equation (3); that is

$$K_r > \frac{\alpha}{(2+H)\,(N_{Re})^{1+\beta}_{\theta,e,c}} \quad (6)$$

where the shape factor H and the constants α and β of the shear stress relation depend on the velocity profile within the boundary layer at the onset of reverse transition. For a one-seventh power profile $\alpha = 0.0128$, $\beta = 1/4$ and $H = 1.286$. Substitution in Equation (6) yields Equation (3). For a one-eleventh power profile (*22*), $\alpha = 0.00655$, $\beta = 1/6$, and $H = 1 + (2/11) = 1.18$ (*21, 22*). Substitution in Equation (6) yields

$$K_r > \frac{0.00206}{(N_{Re})^{7/6}_{\theta,e,c}} \quad (7)$$

which upon combination with Equation (5) (or Figure 1) leads to the lower curve presented in Figure 2. Accordingly (Figure 2), the effect of the initial velocity profile on the onset of reverse transition is minor relative to that of the free-stream turbulence intensity, particularly at the lower turbulence levels.

It should be noted that the acceleration parameter K_r in Equations (1) to (3), (6), and (7) and in Figure 2 is for a plane accelerating flow. For an axisymmetric accelerating flow, an additional term is required in the original integral momentum equation, and by following the same procedure which leads to Equation (3), we obtain

$$K_r \equiv \left[\left(\frac{\nu_o}{U_e^2}\right)\frac{dU_e}{dX} + 0.304\left(\frac{\nu_o}{U_e R}\right)\frac{dR}{dX}\right] > \frac{0.0039}{(N_{Re})^{5/4}_{\theta,e,c}} \quad (8)$$

for which $(dR/dX) \to 0$ or $R \to \infty$ is a special case leading to Equation (3).

According to Equation (8), the axisymmetric acceleration parameter consists of two terms of opposite signs when applied to the converging section of an axisymmetric nozzle; that is, axisymmetry has an offsetting effect on the plane acceleration parameter. However, the transitional Reynolds numbers $(N_{Re})_{\theta,e,c}$, for the axially symmetrical flow are higher than those for the plane flow (*18*), so that an axisymmetric analogue of Equation (4) has to be employed in conjunction with Equation (8) to derive a complete reverse transition criterion for an axisymmetric accelerating flow similar to that presented in Figure 2 for a plane accelerating flow. However, the curves of Figure 2 should serve as good approximation for axisymmetric flow in large diameter nozzles ($R \to \infty$).

The results presented in Figure 2 appear consistent with recent experimental results. For example, Schraub (*8*) used a tracer technique to count the frequency at which turbulence bursts leave the wall at various rates of free-stream acceleration. The burst frequency was found to decrease continuously with increased values of the parameter $Z = (\nu_e/u_e^2)\,(du_e/dx)$. The free-stream turbulence intensities at the start of convergence were reportedly below 1%, and for this condition a decrease in bursting was observed to start when $Z > 0.5$ (10^{-6}).

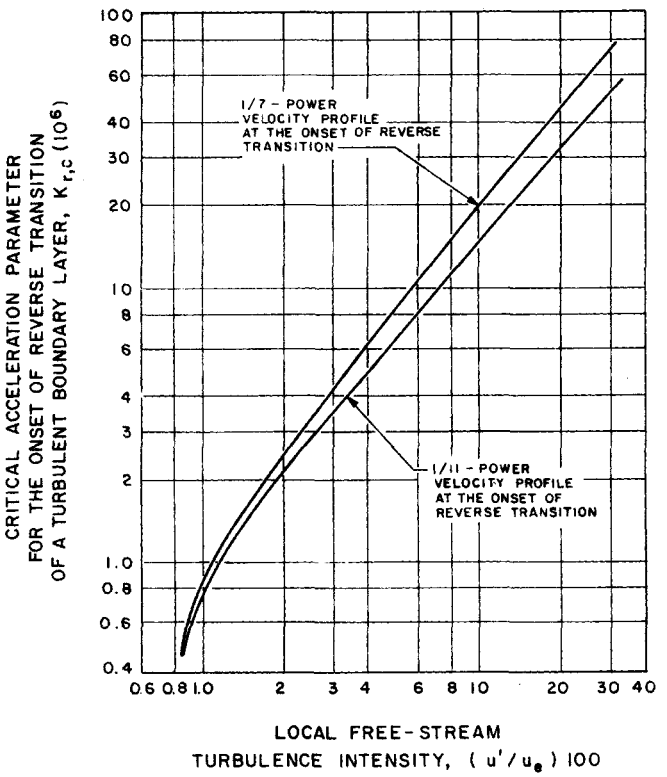

Fig. 2. Effect of free-stream turbulence on the onset of reverse transition of a turbulent boundary layer.

According to Figure 2, this should have been the case; that is, a critical value of $0.5(10^{-6})$ has to be exceeded when the free-stream turbulence intensity is approximately 0.85%.

As the acceleration parameter increased (8), the turbulence bursting frequency decreased to a minimum of nearly zero for $Z > 3.5(10^{-6})$. The decrease in bursting was almost linear with Z, revealing a rather rapid response of the boundary layer to local changes in Z. However, a certain delay or lag was evident in the effect of Z on the burst frequency, particularly towards the end of the laminarization process. For example (8), the point at which Z reached a maximum value of $3.5(10^{-6})$ was approximately 6 in. upstream of the point at which the burst frequency was at its minimum. This seems reasonable, as the average turbulence at any point in the boundary layer is affected by conditions upstream of the point considered. However, while a lag exists in realizing the full potential of the reverse transition (or laminarization) phenomenon, there seems to be no significant lag in the onset of reverse transition as soon as the acceleration parameter exceeds its critical value. This simplifies the use of Figure 2 for predicting the onset of reverse transition of a turbulent boundary layer. However, to realize the full potential of laminarization in actual design applications, allowance has to be made for a lag between the point at which the critical value of the acceleration parameter was exceeded and the point at which the corresponding potential of heat transfer reduction is fully realized. This will be reflected by the correlation of experimental results to be presented herein.

APPARATUS AND PROCEDURES

Test Sections

Rectangular flow channels were designed to provide a wide variation in the acceleration parameter K_T. This was accomplished by variation in wall convergence angle (45, 60, and 70 deg.) and overall flow area contraction ratio (17.5 to 58.0). Further variation of K_T for a given test section was accomplished by variation in the operating stagnation pressure (200 to 500 lb./sq.in.abs.). Thus, K_T varied from $1.15(10^{-6})$ to $8.2(10^{-6})$.

All test sections consisted of an instrumented converging wall opposite to an adjustable nonconverging plate (Figure 3). The channel size and contraction ratio were varied by positioning the nonconverging plate at various heights above the converging wall. The channels were ½ in. wide in all cases.

With the inlet height of the channel being on the order of 2.5 in. and the throat height being in the range of 0.043 to 0.152, a constant chanel width of ½ in. corresponded to an inlet aspect ratio of 1/5 and a throat aspect ratio of 3.3 to 12.5.The relatively low aspect ratio at the inlet is not believed to have compromised the heat transfer results along the converging wall because of the flow separation at the start of steep convergence due to the sharp turning of the flow (12).

All converging walls had the same radius of curvature at the throat (Figure 3). The 70-deg. ramp also had the same radius of curvature at the start of convergence. Each converging wall consisted of a 0.011 in. thick stainless steel sheet bent around the corners of grooved, aluminum ramp pieces. The 1/16 in. deep by 3/8 in. wide grooves in the ramp pieces provided routing space for thermocouples, which were fastened to the back side of the calorimeter sheet. Thermocouple spacing was ⅜ in. for the 45-deg. ramp, ¼ in. for the 60-deg. ramp, and ¼ in. for the 70-deg. ramp, starting in each case one-half space downstream of the start of convergence. Twelve, fourteen, and fifteen thermocouples were installed in the 45-, 60-, and 70-deg. ramps, respectively. Each test section was bolted to an adapter flange housing a turbulence inducing grid. Bypass orifices upstream of the turbulence grid controlled the stagnation pressure within the test section.

Instrumentation

Premium grade, Chromel-Alumel, 0.005-in. diameter thermocouple wire was used to measure gas and converging wall temperatures. The time transient outputs from inlet gas and wall temperature thermocouples were gathered by a Beckman 210 digital data acquisition system in conjunction with a magnetic tape recording facility. The temperature data from each of fifty channels could be sampled every 0.0117 sec. and recorded in digital form with an accuracy of approximately one part in 4,000.

Wiancko pressure transducers, calibrated by using Heise gauges, were used to monitor and record test section and flow facility pressures before and during the tests. The pressures were recorded on continuous strip charts by using Honeywell-Brown recorders operating at ¼ in./sec. chart speed and having ½% full-scale calibation accuracy.

Hot-Gas Facility

The hot-gas facility used for this study was capable of supplying gaseous nitrogen at flow rates up to 3.5 lb./sec., temperatures up to 1,100°F., and pressures up to 1,000 lb./sq.in. gauge for a time duration of 4 sec. Lower flow rates allowed correspondingly longer flow durations.

The facility consisted of a pressure regulated, ambient temperature nitrogen supply and an electrically heated, pebble bed type of regenerative heat exchanger. A 2-in. diameter, double burst diaphragm acted as a hot-gas valve at the outlet of the heat exchanger. This valve had an effective opening time of 1 msec. A 1 ft.-long, 2-in. pipe spool at the outlet of the hot-gas valve adapted the

various test sections employed.

The mass flow rate of the gas was controlled by the main pressure regulator in conjunction with flow bypass orifices. Flow rates were calculated from measured gas pressures and temperatures and known exit throat areas.

Turbulence Grids

Turbulence grids were designed (*11*) to induce turbulence intensities of 11, 7, and 1.75% at the start of a 45-deg convergence. The grids were at a fixed position, and as the convergence angle of the test section was increased, the distance between the grid and the start of convergence increased. This resulted in a slight decay of turbulence intensity at the start of convergence as the convergence angle was increased, for example, from 11 to 10, 7.0 to 6.4, and 1.75 to 1.6 as the convergence angle was increased from 45 to 70 deg.

Data Reduction

Digitized temperature data, which were available in analogue form on brush recording charts, were examined to determine proper time slices for determination of heat transfer coefficients and adiabatic (steady state) wall temperatures. The digitized data for the chosen time slices were processed for each run by using an unpacking and temperature scaling program to obtain the temperature values. On the average, twenty data slices were taken per run.

Initial values of heat transfer coefficients were evaluated through an elementary heat balance between the gas and the wall, neglecting conduction and radiation heat losses and assuming a thermally thin wall; that is

$$h(T_{aw} - T_w) = \rho_w c_{p,w} \xi (dT_w/d\theta) \qquad (9)$$

where T_{aw} is the measured (corrected) steady state wall temperature and T_w is a measured wall temperature at time θ. Integrating over a time period θ for which h can be taken as constant and solving for h, we get

$$h = \frac{\rho_w c_{p,w} \xi}{\theta} \ln\left[\frac{T_{aw} - T_{w,0}}{T_{aw} - T_{w,1}}\right] \qquad (10)$$

where the time increment θ has to be long enough to meet the assumption of a thermally thin wall and yet short enough to stay within the heating period and meet the assumption of constant h; that is, variable heating rates require variable time increments. Upon consideration of these requirements, a procedure was worked out whereby the first half second of the run was used for all thermocouples at the high stagnation pressures (400 to 500 lb./sq.in.abs.) and also for the thermocouples in the throat region (stations 9 and above) at the medium and low pressures (300 and 200 lb./sq.in.abs., respectively). For the thermocouples at the early part of convergence (stations 1 through 8), the first 1 sec. of the run was used at the medium and low stagnation pressures. This procedure provided comparable precision limits for h on a station-to-station basis. Smaller time increments had a minor effect on the resulting heat transfer coefficients.

The heat transfer coefficients thus calculated were subsequently used for lateral-conduction error analysis by using the fin-conduction equation. The correction was on the order of 10 deg. for a measured wall temperature of 920°F., and the corrected adiabatic wall temperature was in excellent agreement with the recovery temperature derived from the measured gas temperature. Axial conduction and thermal radiation were also checked and found negligible.

Data Presentation and Correlation

The local heat transfer coefficients were plotted in the form of $(N_{Nu})_r/(N_{Pr})^{0.4}$ vs. $(N_{Re})_r$ on log-log coordinates. The Nusselt and Reynolds numbers were based on the local equivalent diameter, with the properties ρ, μ, and k taken at the arithmetic average of the adiabatic wall temperature and the mean wall temperature for the time period θ. Initial plots were for a given convergence angle at common flow-area contraction ratios. Representative levels of heat transfer in the turbulent and laminar boundary-layer flow regimes were superimposed on the data as guidelines for the progress of reverse transition.

Turbulent boundary-layer heat transfer levels were represented by those of Colburn (*24*), Bartz (*25*), and Talmor (*2*); that is

$$(N_{Nu})_r/(N_{Pr})^{0.4} = 0.023\,(N_{Re})_r^{0.8} \qquad (11)$$

$$(N_{Nu})_r/(N_{Pr})^{0.4} = 0.026\,(N_{Re})_r^{0.8} \qquad (12)$$

and

$$\frac{(N_{Nu})_r}{(N_{Pr})^{1/3}(N_{Re})_r^{0.80}} = 0.0375\left[\frac{\gamma - 1}{2\gamma}\right]^{0.20} \frac{(d_h/z)^{0.20}}{(P_e/P_o)^{1/5\gamma}}\left[-\frac{d(P_e/P_o)}{dx}\right]^{0.20}\left(\frac{T_r}{T_o}\right)^{0.6m} \qquad (13)$$

respectively. Equations (11) and (12) are special cases of Equation (13) for accelerating flow in rectangular channels. However, the use of Equation (13) requires knowledge of local pressure-ratio gradients. As local pressure measurements were not taken, Equation (13) was used only where a one-dimensional isentropic pressure profile was deemed applicable, for example, at the early portion of convergence.

Local laminar heat transfer levels were calculated through an internal flow analogue of an external flow relation (*2, 26*); that is

$$\frac{(N_{Nu})_r}{(N_{Pr})^{1/3}(N_{Re})_r^{1/2}} = 0.35\left(\frac{T_r}{T_o}\right)^{\frac{1-m}{2}}\left(\frac{P_o}{P_e}\right)^{1/2} \frac{d_h^{1/2} z^{1/4}}{\left[\int_0^x \left(\frac{P_e}{P_o}\right)^{\frac{m(\gamma-1)+1}{\gamma}} z^{1/2}\, dx\right]^{1/2}} \qquad (14)$$

where

$$z = \left(\frac{P_e}{P_\infty}\right)^{\frac{\gamma-1}{\gamma}}\left[\left(\frac{P_o}{P_e}\right)^{\frac{\gamma-1}{\gamma}} - 1\right]$$

Equation (14) was used in the higher area ratio range, where a one-dimensional isentropic pressure distribution could be assumed. For the throat region, the level of Brinsmade and Desmon (*27*) was superimposed on the data; that is

$$(N_{Nu})_r/(N_{Pr})^{0.4} = 0.290\,(N_{Re})_r^{0.5} \qquad (15)$$

Equation (15) represents data obtained at the sonic point of a solid propellant combustion chamber, and it is also supported by recent throat heat transfer results with various propellant combinations at low stagnation pressures (*28*).

To combine and correlate transitional heat transfer data at various convergence angles, the acceleration parameter K_r [defined by the left side of Equation (2)] had to be calculated for all test sections (Figure 3) and all locations. The required gas dynamics data [P_o/P_e, N_{Ma}, $-d(P_e/P_o)/dx$] were obtained from one-dimensional isentropic flow relations, and a digital computer program, RETRAN, was written to evaluate the acceleration parameter. The program determined the local slope

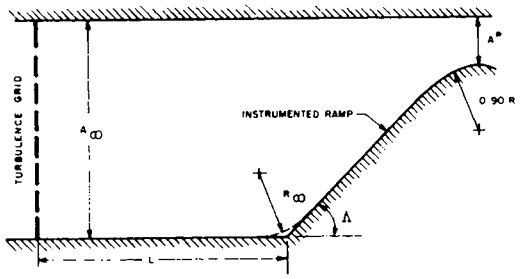

CONFIGURATION	Λ	A_∞	A^*	L	R_∞	ϵ_∞
a	45	2.58	0.120	6.24	—	21.5
b	60	2.59	0.0825	7.30	—	31.4
c	60	2.66	0.152	7.30	—	17.5
d	70	2.56	0.114	7.10	0.90	22.4
e	70	2.58	0.147	7.10	0.90	17.6
f	70	2.49	0.043	7.10	0.90	58.0
g	70	2.51	0.094	7.10	0.90	26.7

Fig. 3. Test section schematic.

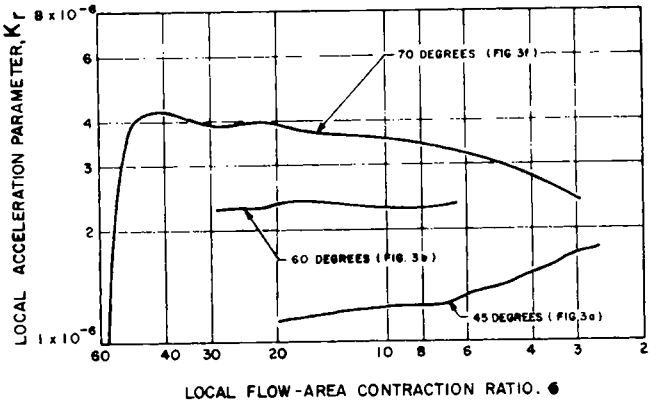

Fig. 4. Typical variation of the acceleration parameter at the various convergence angles.

$-d(P_e/P_o)/dx$ by differentiating the relations $(P_e/P_o) = f(\epsilon)$ and $\epsilon = g(x)$ and by combining the derivatives. Values of local temperature ratios and Reynolds numbers were input variables, based on actual geometrical and operating conditions. The use of one-dimensional isentropic flow functions did not introduce any correlation error because the acceleration parameter eventually used for correlation of local heat transfer data was that existing at or near the start of convergence where the assumption of one-dimensional isentropic flow conditions is valid. This choice of an upstream acceleration parameter for correlating downstream heat transfer measurements is consistent with the observed lag between the point at which K_T was maximum and the point where the wall turbulence burst frequency was minimum (8). However, the exact location of the effective acceleration parameter may sometimes need special consideration.

For example, typical computer plots of K_T vs. ϵ at the various convergence angles and comparable stagnation pressures (400 to 500 lb./sq.in.abs.) are shown in Figure 4. For the convergence angles of 45 and 60 deg., the curves are relatively flat near the start of convergence so that the value of the effective acceleration parameter for correlating downstream heat transfer measurements is not sensitive to its location relative to the start of convergence. However, at a convergence angle of 70 deg., there is a steep rise in K_T over a very small change in area ratio immediately after the start of convergence. This is attributable to the radius of curvature at the start of convergence which the 45- and 60-deg. ramps did not have. Therefore, for consistency, the value of K_T at the end of the steep rise was chosen for correlating the downstream transitional heat transfer data at a convergence angle of 70 deg. The effective acceleration parameters $(K_{T,x})$ thus chosen were in the range of $1.15(10^{-6})$ to $8.2(10^{-6})$ at the convergence angle of 70 deg. (Figures 3*d* to 3*g*), $1.5(10^{-6})$ to $4.8(10^{-6})$ for the convergence angle of 60 deg. (Figures 3*b*, 3*c*) and $1.15(10^{-6})$ to $2.2(10^{-6})$ at the convergence angle of 45 deg. (Figure 3*a*).

RESULTS AND DISCUSSION

Local heat transfer measurements were taken in a matrix of forty-five runs at three stagnation pressures covering a span of 200 to 500 lb./sq.in.abs., three turbulence levels at the start of convergence (1.6 to 11%), and five overall contraction ratios (17.5 to 58) at three convergence angles (45, 60, and 70 deg.). Inlet Mach numbers ranged from 0.01 to 0.035 for the various test sections.

The data were first plotted in the form of $(N_{Nu})_T/(N_{Pr})^{0.4}$ vs. $(N_{Re})_T$ at common area ratios and convergence angles. The results suggested the use of $K_{T,x}$ as a correlating parameter.

For example, pertinent results for two channels at a convergence angle of 70 deg. are given in Figure 5. At an area ratio of 17.6 which is the start of convergence for the solid points, turbulent separation is apparent. However, the open points obtained further downstream of the start of convergence at a higher average acceleration parameter follow a lower heat transfer level. At the next station ($\epsilon = 14.0$), both sets of data appear merged into a laminarized level, and at $\epsilon = 9.5$, the two sets of data are again separated. In reference to the previous station ($\epsilon = 14.0$), the solid points for which the average acceleration parameter is lower seem to have moved upward, while the open points (at a higher average $K_{T,x}$) seem to have moved downward to a somewhat lower level. Towards $\epsilon = 7.7$, the solid points have shifted to an apparently turbulent level which is sustained at area ratios of 5.7 and 3.9 as well. At $\epsilon = 1.2$, the solid points seem reverted to the original pseudo laminar heat transfer level observed at $\epsilon = 14.0$, thus suggesting a repeated process of laminarization.

Meanwhile, the open points are sustaining their pseudo laminar level at area ratios of 7.7 and 5.7 (Figure 5). Towards $\epsilon = 3.9$, further laminarization is evident at the higher acceleration parameters (open points) and at the low and intermediate Reynolds numbers (300,000 and 400,000 at $\epsilon = 5.7$). At the high Reynolds number (520,000 at $\epsilon = 5.7$), no further laminarization is realized. This results in the onset of a high slope (> 1.0) for the open points at $\epsilon = 3.9$, which is fully established at $\epsilon = 1.2$ and 1.0 with Reynolds numbers approaching $1(10^6)$.

The main feature of the results given in Figure 5 is a diversified two-stage laminarization process. In one case (solid points), it consists of two repeated reverse transitions with a forward transition inbetween. In the other case (open points), the first stage of reverse transition consists of suppression of Nusselt numbers to a pseudo laminar heat transfer level higher than typical for a laminar boundary layer. This level is sustained for some distance along the converging wall before the onset of a second-stage reverse transition process, preferentially at the lower Reynolds numbers leading to high slope (> 1.0) heat transfer lines towards the end of convergence. The observation of such a two-stage reverse transition process is at least qualitatively consistent with basic

boundary-layer measurements (*6, 8*), and the attainment of high slope heat transfer lines at throat Reynolds numbers approaching $1(10^6)$ is consistent with experimental heat transfer results with high temperature combustion products in similar channels (*4*).

It is rather revealing to note that at $\epsilon = 1.2$ the upper end of the open points for which $K_{r,x} = 1.6(10^{-6})$ tends to merge with the solid points for which $1.14\ (10^{-6}) < K_{r,x} < 2.3(10^{-6})$. The lower end of the open data points where $K_{r,x} = 3.1(10^{-6})$ is outside this range, tending to pull away from the solid points into a deeply laminarized state. Thus, what appears to be a lack of correlation of an apparent effect of channel size is actually an acute effect of the acceleration parameter. Furthermore, a systematic mild effect of the free-stream turbulence at the start of convergence is evident at area ratios down to 3.9, particularly at the low Reynolds numbers. This is a characteristic of a laminarized or transitional state (*29*). The absence of such effect near the throat is apparently due to appreciable decay in turbulence intensity upstream of the throat.

Generally, the heat transfer results were not significantly affected by the free-stream turbulence intensity at the start of convergence. This tends to indicate that regardless of its level at the start of convergence, the free-stream turbulence has decayed to common low values along the converging wall. These could not be calculated, since the effect of assymmetric contraction on grid induced turbulence is yet to be investigated (*30*). Furthermore, the well-observed flow separation at the start of steep convergence (*12*) isolates the converging wall from the effect of free-stream turbulence at the start of convergence. Therefore, the apparently negligible effect of upstream turbulence intensity on heat transfer along the converging wall (at $K_{r,x} > K_{r,c}$) should not be construed to imply lack of influence of free-stream turbulence on the onset of reverse transition (Figure 2). Alleviation of flow separation at the start of convergence and measurements of local free-stream turbulence are required for further elucidation of the phenomena involved.

Data Correlation

Data for various test sections were combined to yield curves of constant $K_{r,x}$ at various area ratios. Since the free-stream turbulence intensity at the start of convergence was found to have a minor effect (if any) on the heat transfer coefficients along the converging wall, no further distinction was made relative to the presentation of data obtained at various free-stream turbulence intensities at the start of convergence. However, each range of $K_{r,x}$ was assigned a symbol on each constant-area-ratio plot, and alternate open and solid points were used for contrast. While the symbols are individually identified on each plot, they are not transferable from figure to figure.

The reference levels represented by Equations (11) to (15) were again superimposed on the data. However, for the case of Equations (13) and (14) which yield individual levels for each of the test sections employed, an average level was superimposed on the combined data of various test sections.

First-stage laminarization paths are given in Figure 6 at area ratios of 18 to 19.4. A typical path is of negative slope indicating a sharp decrease in Nusselt number upon a mild increase in Reynolds number at a constant $K_{r,x}$. Referring to the definition of the latter [left side of Equation (2)], an increase in Reynolds number at a constant $K_{r,x}$ implies a simultaneous increase in pressure-ratio gradient and/or a decrease in Mach number so as to compensate for the increased mass velocity.

While reverse transition is evident at all values of $K_{r,x}$ at $18 < \epsilon < 19.4$ (Figure 6), the onset of forward transition back to a turbulent boundary layer is apparent downstream at $11.0 < \epsilon < 12.6$ (Figure 7) for $K_{r,x} \leq 2.6(10^{-6})$. This is reflected by the curling of paths at $K_{r,x} \leq 2.6(10^{-6})$, that is, the lower ends of the paths (close to a laminar level) tending to follow a higher transitional slope (> 1.0) as $(N_{Re})_r$ is increased, while the upper ends of the paths (in the turbulent boundary-layer regime) follow lower slopes on the order of 0.8. The net result is curling, or the formation of an inflection point on the laminarization path. On one side of the inflection point, higher $K_{r,x}$ at a given $(N_{Re})_r$ results in lowering the heat transfer rate (lower half of the curled paths). On the other side of the inflection point (upper half of the curled paths) higher $K_{r,x}$ at a given $(N_{Re})_r$ tends to increase the Nusselt number which is closer to a characteristic of a turbulent boundary layer. Thus, the results in Figure 6 represent the end of a first-stage laminarization process, at least for $K_{r,x} \leq 2.6(10^{-6})$.

The curling phenomenon for $K_{r,x} \leq 2.6(10^{-6})$ first noticed at $16.0 < \epsilon < 16.5$, if indeed attributable to for-

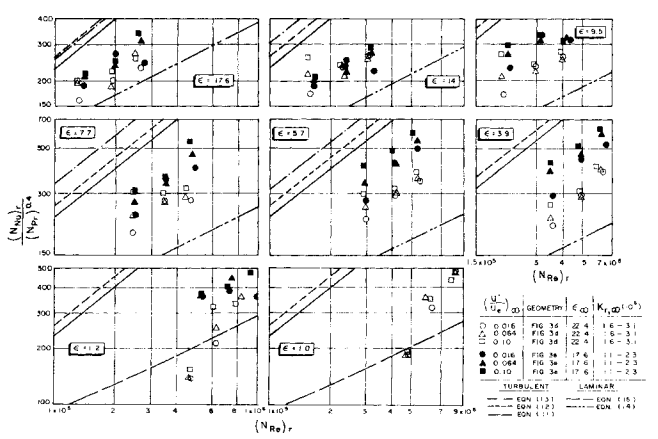

Fig. 5. Local heat transfer results at a convergence angle of 70 deg. and two overlapping ranges of the acceleration parameter $K_{r,\infty}$.

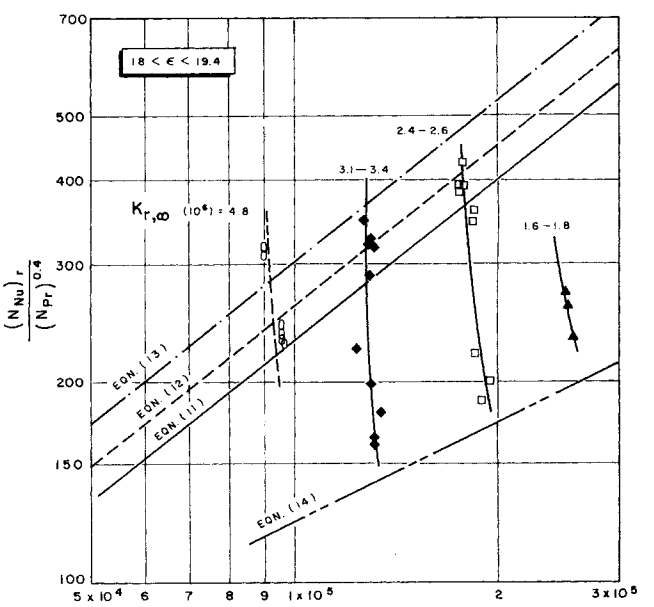

Fig. 6. Laminarization paths at $18 < \epsilon < 19.4$ with $22 < \epsilon_x < 30$; Nusselt numbers decrease with increased Reynolds number at constant $K_{r,\infty}$

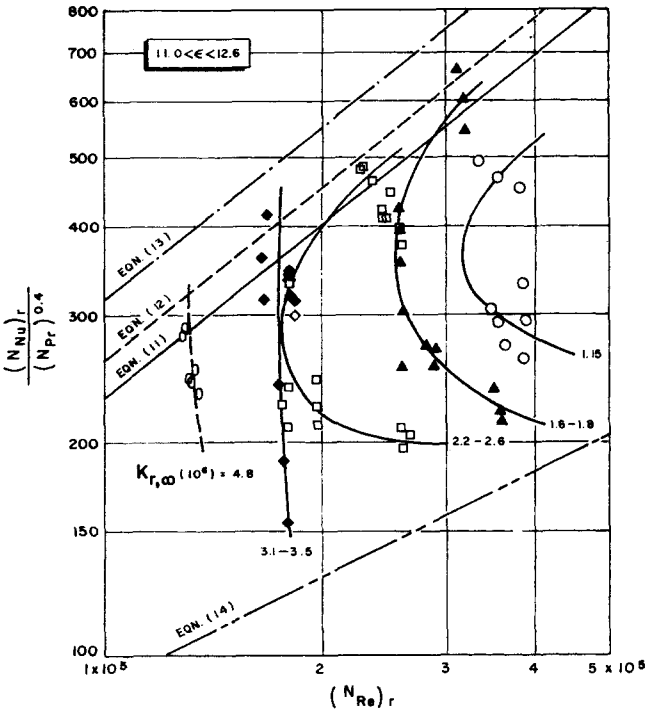

Fig. 7. Laminarization paths at $11.0<\epsilon<12.6$ with $18<\epsilon_x<30$; curling of paths at $K_{r,\infty}<2.6(10^{-6})$ is due to forward transition at their lower ends while their upper ends follow lower turbulent slopes.

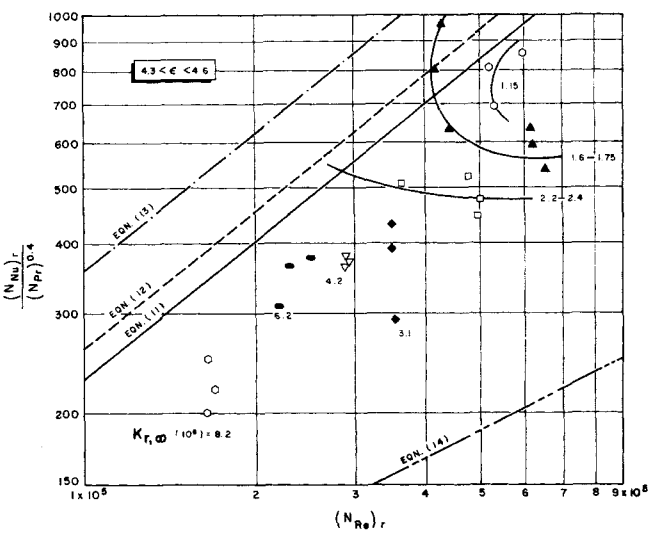

Fig. 9. Laminarization paths at $4.3<\epsilon<4.6$ with $18<\epsilon_x<58$; curling tends to disappear as a turbulent boundary-layer flow regime is approached.

ward transition at the lower ends of the laminarization paths, should be more pronounced at positions downstream and should eventually propagate to higher values of $K_{r,x}$. This is supported by the results presented in Figure 8 for area ratios of 7.3 to 8.0. Curling is appreciable for $K_{r,x} < 3.5(10^{-6})$ and mild at $K_{r,x}$ of $5.6(10^{-6})$ and $8.2(10^{-6})$ (Figure 8). Subsequently, at $4.3 < \epsilon < 4.6$ (Figure 9), the ultimate in curling (or forward transition) seems to have been reached. What used to be the lower end of a laminarization path is now catching up with its upper end, resulting in a mildly negative slope for the path, for example, that shown for $2.2(10^{-6}) < K_{r,x} < 2.4(10^{-6})$ in Figure 9.

One would expect the next step to consist of a complete shift to a positive turbulent slope of 0.8. Instead, the onset of a second-stage laminarization process is revealed by the heat transfer results at the next station ($3.0 < \epsilon < 3.9$, Figure 10). This stage of laminarization is rather persistent, penetrating deeper towards a laminar state at $1.7 < \epsilon < 2.7$ (Figure 11) with curling of paths evident at the lower values of $K_{r,x}$ ($\leq 1.8 \times 10^{-6}$) only. Finally, at $1.0 < \epsilon < 1.5$ (Figure 12), the ultimate in reverse transition seems to have been reached. Curling has disappeared, and clear constant $-K_{r,x}$ laminarization paths are evident in the entire range of $K_{r,x}$ investigated. All paths seem to lead to a laminar boundary-layer heat transfer level which is obviously lower than that of Equation (15) and lower than that apparent for the first stage of laminarization (Figure 6); that is, the second stage is more decisive despite the existence of forward transition between the two stages of reverse transition.

The constant $-K_{r,x}$ laminarization paths presented in Figures 6 to 12 should not be confused with throttling paths obtainable upon wide variation of stagnation pressure (or Reynolds number) with a given channel geometry. In this case, $K_{r,x}$ varies simultaneously with $(N_{Re})_r$, so that the throttling path consists of continuous shifting from one laminarization path to another resulting in a positive slope for $(N_{Nu})_r/(N_{Pr})^{0.4}$ vs. $(N_{Re})_r$. At least for the throat region, the slope of the throttling path varies with the Reynolds number range of operation (4).

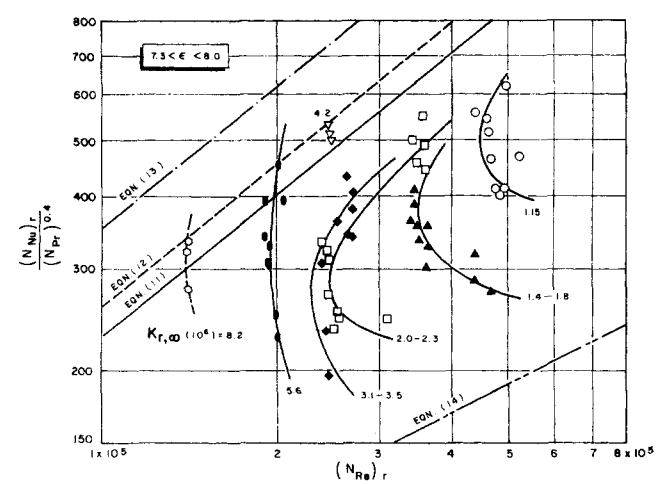

Fig. 8. Laminarization paths at $7.3<\epsilon<8.0$ with $17<\epsilon_x<58$; curling appreciable at $K_{r,\infty} \leq 3.5(10^{-6})$.

Application to Design

Reverse transition is most helpful for suppression of heat transfer rates in critical (difficult to cool) regions, for example, the throat region of combustion chambers. The induction of reverse transition in the vicinity of the sonic point requires careful contouring of the converging wall upstream (not necessarily through the convergence angle) so as to ensure that the acceleration parameter is favorable for reverse transition. This will require consideration of local free-stream turbulence intensities in accordance with Figure 2. Once the critical value of the acceleration parameter is exceeded at the proper location relative to the sonic point, for example, at the start of convergence for converging wall lengths on the order of 4 in., knowledge of the resulting heat transfer coefficients is required.

The results presented in Figures 6 to 12 are directly applicable for determination of transitional heat transfer coefficients along plane converging walls. However, a complicating factor may be introduced by the curling of

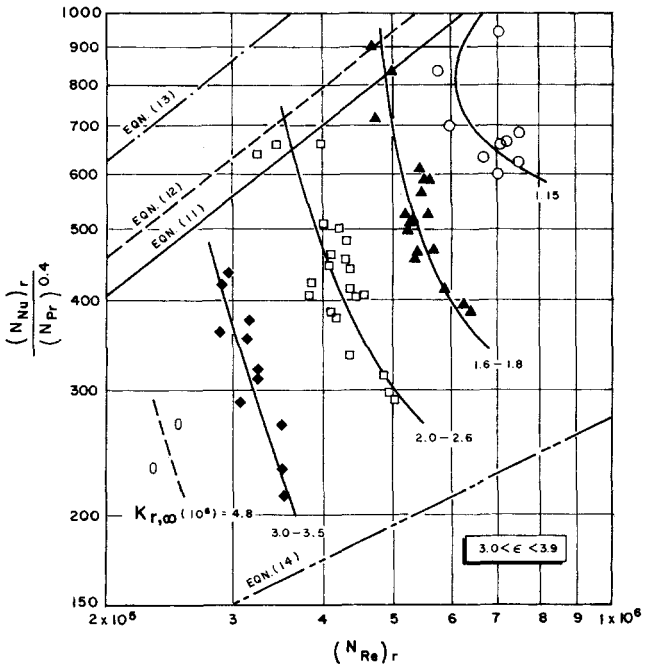

Fig. 10. Second-stage laminarization at $3.0<\epsilon<3.9$ with $17<\epsilon_{\infty}<30$.

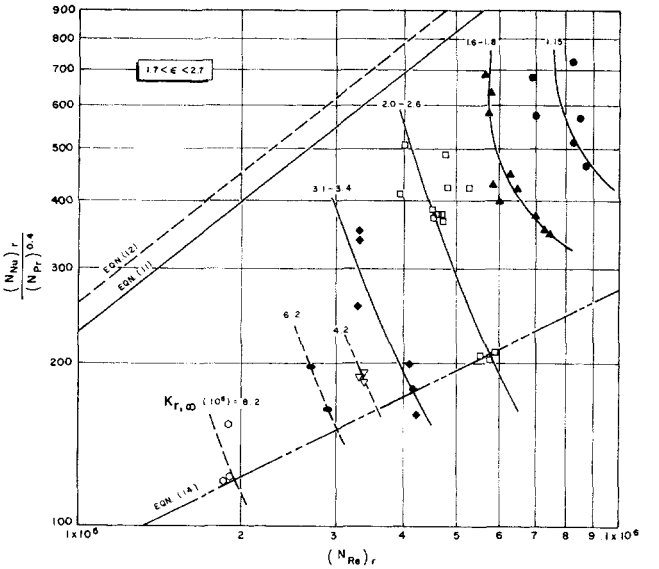

Fig. 11. Laminarization paths at $1.7<\epsilon<2.7$ with $17<\epsilon_{\infty}<58$.

laminarization paths in some cases, particularly if Figure 2 is not consulted.

The curled constant $-K_{r,x}$ laminarization path represents a double valued function. For example (Figure 8), at a constant value of $(N_{Re})_r$, two values of $(N_{Nu})_r/(N_{Pr})^{0.4}$ are sometimes possible, one on each side of the inflection point of the curve, one close to a turbulent value, and the other close to a laminar value. The clue as to a proper choice lies in Figure 2 by determining whether the acceleration parameter under consideration is above the critical for reverse transition. Should $K_{r,x}$ be higher than $K_{r,c}$ (Figure 2), the lower of the two values of $(N_{Nu})_r/(N_{Pr})^{0.4}$ is appropriate for design.

It is obvious that this procedure is sensitive to the assumed level of local free-stream turbulence when the reverse transition criterion presented in Figure 2 is applied. The effect of high acceleration rates (particularly when not symmetrical) on free-stream turbulence is hardly predictable and yet to be investigated. The only saving grace at this time is that in the region of immediate interest, that is, the throat region, all laminarization paths are single valued (Figure 12).

CONCLUSIONS AND RECOMMENDATIONS

The onset of reverse transition of a turbulent boundary layer is strongly affected by the free-stream turbulence intensity, with a mild effect of the initial velocity profile within the turbulent boundary layer being noted. Analytical results derived by combining a previously developed reverse transition criterion (2) with a theory of forward transition (18) indicate that for a one-seventh power velocity profile at the onset of reverse transition, the acceleration parameter has to exceed a value of $1(10^{-6})$ to induce reverse transition at a free-stream turbulence level of 1.1%, while a value of $4.4(10^{-6})$ has to be exceeded at a free-stream turbulence intensity of 3%. For a one-eleventh power velocity profile at the onset of reverse transition, the critical values are $0.91(10^{-6})$ and $3.5(10^{-6})$ at free-stream turbulence levels of 1.1 and 3%, respectively. These results, consistent with experimental results, suggest that a fast decay in free-stream turbulence prior to or during the early stage of convergence should be highly favorable for the onset of reverse transition.

The local heat transfer coefficients along plane converging walls are strongly affected by the acceleration parameter at or near the start of convergence particularly when the critical value for reverse transition has been exceeded. This is consistent with the observed lag between the point at which the acceleration parameter is maximum and the point at which the full potential of laminarization is realized (7, 8). Experimental results of this study with $1.15(10^{-6}) < K_{r,x} < 8.2(10^{-6})$ and free-stream turbulence intensities of 1.6 to 11% at the start of convergence indicate a two-stage reverse transition process along the converging wall with a forward transition in between. The second stage of laminarization is more effective, leading to heat transfer levels much further suppressed below those typical for turbulent boundary layers.

The acceleration parameter at the start of convergence is a powerful tool for correlating local heat transfer rates at common flow-area contraction ratios, at least for the converging wall lengths employed (on the order of 4 in.). This is reflected by the establishment of constant $-K_{r,x}$ laminarization paths having negative slopes of $(N_{Nu})_r/(N_{Pr})^{0.4}$ vs. $(N_{Re})_r$ at common local area ratios. However, no correlation is evident relative to the free-stream

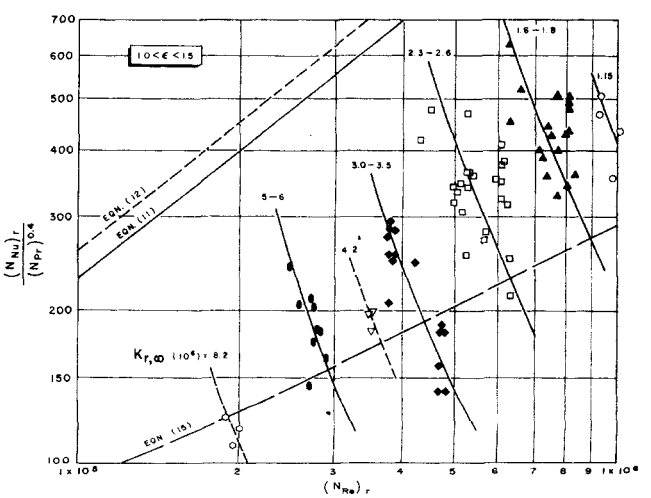

Fig. 12. Laminarization paths at $1.0<\epsilon<1.5$ with $17<\epsilon_{\infty}<58$.

turbulence intensity at the start of convergence, as it had a negligible effect on the local heat transfer coefficients even in the laminarized state. Apparently, the free-stream turbulence decayed along the converging wall to common low values, regardless of its initial intensity at the start of convergence.

Local measurements of free-stream turbulence intensity along converging walls at various rates of acceleration are required to alleviate the designer's problem of assuming a turbulence level when applying the reverse transition criterion and the heat transfer results presented herein.

ACKNOWLEDGMENT

The authors wish to extend their appreciation to John Sabol for his vital data reduction effort, to Joe Myers for his experimental support, and to L. W. Carlson for his help in the experimental setup.

NOTATION

A = local channel height, Figure 3
A^* = throat height, Figure 3
C = constant in the relation $(N_{Nu})_x = C(N_{Re})_x^n$
c_p = specific heat at constant pressure
d_h = equivalent diameter, four times the ratio of wetted area to wetted perimeter
H = shape factor, Equation (6)
h = heat transfer coefficient, Equation (9)
K_T = acceleration parameter for compressible flow defined by the left sides of Equations (1) and (2)
k = thermal conductivity
L = distance between the turbulence grid and the start of convergence, Figure 3
m = gas viscosity-temperature exponent ($\mu \sim T^m$)
N_{Ma} = Mach number
N_{Nu} = Nusselt number = hd_h/k
N_{Pr} = Prandtl number
N_{Re} = Reynolds number = $d_h u\rho/\mu$
n = power in the relation $(N_{Nu})_x = C(N_{Re})_x^n$
P = pressure
R = transformed radius of axisymmetry in Equation (8); radius of wall curvature in Figure 3
T = absolute temperature
U = transformed velocity defined in conjunction with Equation (1)
u = velocity in the x direction
u' = velocity fluctuation in the x direction
X = transformed coordinate system defined in conjunction with Equation (1)
x = distance from the start of convergence along the converging wall
Z = acceleration parameter for incompressible flow = $(\nu_e/u_e^2)\ (du_e/dx)$
z = pressure-ratio function defined in conjunction with Equation (14)

Greek Letters

α, β = constants in the shear stress relation
γ = specific heat ratio
δ = velocity boundary-layer thickness
ϵ = local flow-area contraction ratio
θ = momentum thickness; elapsed time in Equations (9) and (10)
Λ = Pohlhausen parameter, Equation (4); convergence angle, Figure 3
μ = gas viscosity
ν = kinematic viscosity
ξ = wall thickness
ρ = density
τ = shear stress

Subscripts

aw = adiabatic wall
c = critical
e = local conditions along the outer edge of the boundary layer
o = properties at stagnation conditions; at zero time, Equation (10)
r = properties at reference temperature
x = based on x
w = wall
δ = based on δ
∞ = at the start of convergence
1 = at time θ, Equation (10)

LITERATURE CITED

1. Bartz, D. R., "Advances in Heat Transfer," Vol. 2, pp. 1-108, Academic Press, New York (1965).
2. Talmor, Eliyahu, *AIChE J.*, **1**, 127 (1968).
3. Back, L. H., and A. B. Witte, *J. Heat Transfer*, **88**, 249 (1966).
4. Talmor, Eliyahu, *Chem. Eng. Progr. Symposium Ser. No. 82*, **64**, 231 (1968).
5. Back, L. H., P. F. Massier, and R. F. Cuffel, *J. Spacecraft*, **4**, 1040 (1967).
6. Launder, B. E., *Gas Turbine Lab. Rept. No. 77*, Mass. Inst. Technol., Cambridge (1964).
7. Moretti, P. M., and W. M. Kays, *Intern. J. Heat Mass Transfer*, **8**, 1187 (1965).
8. Schraub, F. A., Ph.D. dissertation, Stanford University, Calif. (1965).
9. Back, L. H., and R. A. Seban, "Proceedings of the 1967 Heat Transfer and Fluid Mechanics Institute," p. 410, Stanford Univ. Press, Calif. (June, 1967).
10. Hartnett, J. P., R. C. Birkebak, and E. R. G. Eckert, "International Developments in Heat Transfer," Vol. 4, p. 682, Am. Soc. Mech. Engrs., New York (1961).
11. Carlson, L. W., and Eliyahu Talmor, *Intern. J. Heat Mass Transfer*, **11**, 1695 (1968).
12. Back, L. H., P. F. Massier, and R. F. Cuffel, *AIAA Journal*, **4**, 2226 (1966).
13. Boldman, D. R., J. F. Schmidt, and R. C. Ehlers, *J. Heat Transfer*, **89**, 341 (1967).
14. Talmor, Eliyahu, "Proceedings of the Third International Heat Transfer Conference, Vol. 1, p. 77, Am. Inst. Chem. Engrs., New York (Aug., 1966).
15. Hatton, A. P., and V. A. Eustace, *ibid.*, Vol. 2, p. 34.
16. Ambrok, G. S., *Sov. Phys. Tech. Phys.*, **2**, 1979 (1957).
17. Beckwith, I. E., and J. J. Gallagher, *Natl. Aeronaut. Space Admin. Tech. Rept. R-104* (1961).
18. vanDriest, E. R., and C. B. Blumer, *AIAA Journal*, **1**, 1303 (1963).
19. Wells, C. S., *ibid.*, **5**, 172 (1967).
20. Talmor, Eliyahu, *AIChE J.*, **12**, 1092 (1966).
21. Schlichting, Hermann, "Boundary Layer Theory," McGraw-Hill, New York (1960).
22. Wesoky, H. L., *Natl. Aeronaut. Space Admin. Tech. Note D-3882* (Mar., 1967).
23. Kutateladze, S. S., and A. I. Leontev, "Turbulent Boundary Layers in Compressible Gases," Academic Press, New York (1964).
24. Colburn, A. P., *Trans. Am. Inst. Chem. Engrs.*, **29**, 174 (1933).
25. Bartz, D. R., *Jet Propulsion*, **21**, No. 1, 49 (1957).
26. Talmor, Eliyahu, *Chem. Eng. Prog. Symposium Ser. No. 59*, **61**, 50 (1965).
27. Brinsmade, A. F., and L. G. Desmon, *ibid.*, 88.
28. Schoenman, L., and P. Block, *J. Spacecraft and Rockets*, **5**, 1082 (1968).
29. Junkhan, G. H., and G. K. Servoy, *J. Heat Transfer*, **89**, 169 (1967).
30. Comte-Bellot, Genevieve, and Stanley Corrsin, *J. Fluid Mech.*, **25**, part 4, 657 (1966).

Manuscript received July 26, 1968; revision received October 7, 1969; paper accepted October 8, 1969.